Reliability based optimisation of composite plates under aeroelastic constraints via adapted surrogate modelling and genetic algorithms

Roger Ballester Claret, Ludovic Coelho, Christian Fagiano, Cédric Julien, Didier Lucor, Nicolò Fabbiane

Composite Structures 347 (2024) 118461

Contents lists available at ScienceDirect

Composite Structures

journal homepage: www.elsevier.com/locate/compstruct

Reliability based optimisation of composite plates under aeroelastic constraints via adapted surrogate modelling and genetic algorithms

Roger Ballester Claret [a,b,*], Ludovic Coelho [a], Christian Fagiano [b], Cédric Julien [b], Didier Lucor [c], Nicolò Fabbiane [a]

[a] DAAA, ONERA, Institut Polytechnique de Paris, Châtillon, 92320, France
[b] DMAS, ONERA, Université Paris-Saclay, Châtillon, 92320, France
[c] CNRS, Université Paris-Saclay, Laboratoire Interdisciplinaire des Sciences du Numérique, Orsay, 91400, France

ARTICLE INFO

Keywords:
Aeroelasticity
Lamination parameters
Constrained optimisation
Efficient global optimisation
Reliability-Based Design Optimisation

ABSTRACT

Composite materials are vital in aerospace for their exceptional strength-to-weight ratio. This study delves into reliability-based optimisation of composite plates within aeroelastic constraints, employing an efficient global optimisation method and genetic algorithms. Initial analysis focuses on aeroelastic responses such as limit flutter speed, gust response, and static loads, emphasising maximum strain assessment. To tackle optimisation challenges of composite stacking sequences, a homogenisation technique with lamination parameters is applied. We then formulate a constrained optimisation problem to minimise gust response while meeting flutter and maximum strain constraints. Surrogate models based on conditioned Gaussian Processes are developed for each aeroelastic response, facilitating optimisation within the composite design space. These models, with potential for local refinement, expedite optimal solution identification. Further, we integrate reliability-based optimisation into the framework to determine a robust stacking sequence using genetic algorithms, accounting for random fibre orientation variations. This holistic approach integrates aeroelastic analysis, constrained optimisation, surrogate modelling, and reliability-based optimisation, proving effective in designing reliable, efficient composite structures for aerospace, thus enhancing performance and safety.

1. Introduction

Composite materials have become a cornerstone in engineering fields, particularly in the aerospace sector. Characterised by their exceptional specific strength and stiffness, these materials stand out for their ability to be tailored anisotropically, providing unmatched benefits. This capacity for customisation causes a revolution in structural engineering, enabling ongoing innovations in aerospace design. At the heart of this shift is the principle of aeroelastic tailoring, which plays a pivotal role in leveraging the unique properties of composite materials to optimise the aeroelastic behaviour of an aircraft and, thus, its performance and efficiency. The aeroelastic tailoring has its roots in the middle part of the 20th century with the seminal work by Munk, who adeptly leveraged the natural anisotropy of wood for more efficient propeller designs [1]. Fast forward to the present day, this concept has been further expanded and refined through the use of advanced composite materials, enabling precise control and optimisation of aeroelastic deformations with structures such as the forward-swept wing [2]. These advancements significantly enhance aerodynamic performance and structural integrity, shaping a new paradigm in aerospace design [3].

However, optimal integration of composite materials into intricate aerospace structures requires sophisticated optimsiation techniques, given the high dimensionality of the design space for composite laminates . Numerous methods have been proposed for these optimisation strategies, for instance by introducing genetic algorithms (GA) [4,5] which cope very well with the discrete nature of the fibre orientations in a composite laminate. However, GAs need numerous evaluations of the cost functions which can rapidly augment the computational cost expenses. Another classical class of approaches has been homogenisation techniques [6,7] which allow for the use of a gradient-based optimiser by introducing a convex design space. In this case, the computational cost may be reduced, however the navigation between the different scales can be of high complexity. For instance, the optimisation problems solved within the homogenised space require a stiffness matching problem to retrieve the final optimised laminate [8–10] . Notwithstanding their advantages and disadvantages, both GA and multi-scale optimisation methods for composite materials have traditionally relied on deterministic techniques. Another important aspect is that, given the complex manufacturing processes of layered materials,

* Corresponding author at: DAAA, ONERA, Institut Polytechnique de Paris, Châtillon, 92320, France.
E-mail address: roger.ballester_claret@onera.fr (R. Ballester Claret).

https://doi.org/10.1016/j.compstruct.2024.118461
Received 9 April 2024; Received in revised form 28 June 2024; Accepted 1 August 2024
Available online 5 August 2024

it is crucial to account for the inherent uncertainties [11] as in the final laminate structures when designing critical components [12]. Moreover, those composite components are often subjected to a series of constraints that must be accounted for within the optimisation process. Within the industry, a common approach has been the application of safety factors after a deterministic approach, though this might not always lead to the most efficient solution. An alternative method is Reliability-Based Design optimisation (RBDO), which, despite its higher computational demand, can result in less conservative outcomes. Significant research has been carried out on applying RBDO to composite materials, considering both manufacturing uncertainties [13] and material properties [14].

Given the significant increase in computational cost associated with classical RBDO with direct approaches [15], there is a compelling need to develop optimisation strategies that mitigate these expenses [16–18]. Extensive research has been undertaken to decrease the computational burden [19,20], along with notable advances in the domain of robust design optimisation. A gradient-based approach was introduced by Coelho et al. [21], focusing on the optimisation of composite plates under buckling constraints and using surrogate modelling techniques for uncertainty propagation. Moreover, as seen in Coelho et al.'s work, due to the nature of composite stacking sequences the gradients of reliability-based constraints are not immediately available, making traditional optimisation methods such as gradient descent extremely challenging to apply. However, the surrogate modelling techniques have proven immensely valuable, both in uncertainty propagation, and in deterministic optimisation approaches. Particularly through the Efficient Global optimisation (EGO) method [22] which allows for cheaper uncertainty propagation. For instance, Sabater et al. [23] proposed a two-step strategy leveraging surrogate models for robust design optimisation. Sabater et al. successfully implemented the EGO method as an initial step prior to undertaking robust design, specifically in the optimisation of aircraft airfoils. The EGO approach is an iterative technique which significantly reduces the global optimisation costs of expensive 'black box' functions. Moreover, the EGO process yields a surrogate model which is especially refined near the deterministic solution. Moreover, moving towards constrained optimisation, notable modifications have been made to the EGO algorithm to better accommodate constrained optimisation scenarios [24,25]. This approach illustrates the potential for integrating EGO-based strategies within broader design methodologies, notably with RBDO as proposed in this work.

Building upon these advanced optimisation strategies, the field of aeroelasticity becomes a critical focus, especially when integrating RBDO and surrogate modelling techniques. The complexity of aeroelastic phenomena, such as flutter and divergence, demands rigorous analysis due to their significant sensitivity to the geometric and material properties of aerospace structures. Moreover, aeroelastic phenomena exhibit notable non-linearities which must be accounted for within the optimisation strategies. Following the work of Scarth et al. [26] we aim to extend his RBDO framework to a study case where composite material uncertainties are directly impacting aeroelastic performance. Moreover, similarly to the work by Fabbiane et al. [27], we aim to integrate tailored design strategies that mitigate both static and dynamic aeroelastic loads, thereby improving overall structural resilience and efficiency. By fusing these methodologies within our optimisation framework, we not only aim to advance the precision of aeroelastic assessments but also facilitate a more streamlined and informed design process.

In this study, we present a two-step optimisation strategy tailored for a multi-scale design space, specifically addressing the challenges associated with composite materials. This innovative approach integrates surrogate modelling techniques to manage the high computational demands of RBDO aeroelastic problems. We demonstrate this technique through the optimisation of a composite plate, which serves as a proxy for an aircraft wing, thus subjecting it to aeroelastic phenomena such as divergence, flutter, and wind gust response. The optimisation process begins with the construction of surrogate models using Kriging (KRG) [28], which are then optimised using a modified EGO method. These surrogate models form the basis for executing an RBDO algorithm driven by GA. This approach not only identifies the optimal composite laminate configuration but also incorporates adjustments to handle uncertainties—both from the manufacturing of the composite laminate and from the inherent inaccuracies of the surrogate model itself.

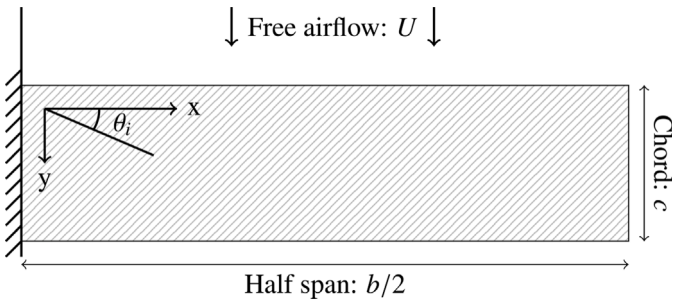

Fig. 1. Composite plate immersed in airflow.

Table 1
Dimensions and material properties.

Parameters	Values
$s/2$ (m)	0.3048
c (m)	0.0762
E_{11} (GPa)	140
E_{22} (GPa)	10
G_{12} (GPa)	5
υ_{12}	0.3
ρ (kg/m^3)	1600
Ply thickness (mm)	0.125

2. Aeroelastic dynamics and composite materials

In this study, we employ a simplified model of a rectangular composite plate to analyse its aeroelastic behaviour. This approach has been used extensively in works like [29,30]. This model, based on the Kirchhoff plate theory and Doublet Lattice Method (DLM) fluid mechanics representation, evaluates the aeroelastic responses while neglecting transverse shear effects. Such a model serves as an initial approximation to understand the aeroelastic behaviour of a wing and is commonly used in aerospace engineering. The plate will be clamped on one edge and free on all the others and submerged into an airflow, as illustrated in Fig. 1. The plate will be constructed from a number of plies N with each ply having a θ_i orientation. The dimensions of the plate and the material properties of the composite plies can be found in Table 1. We will refer to the sequence of plies orientations $\boldsymbol{\theta} = [\theta_1, \theta_2, \dots, \theta_N]$ as stacking sequence. Moreover, within each ply, an orientation error will be considered [31], so the orientation of each ply will be defined as a random variable

$$\theta_i = \bar{\theta}_i + \sigma_{\theta_i} X \tag{1}$$

where $\bar{\theta}_i$ represents the mean objective value of the ith ply orientation, σ_{θ_i} the standard deviation of ith ply and X represents a random variable with a normal distribution with zero mean and unit variance. We note that the random value X will be independent in each of the plies of $\boldsymbol{\theta}$.

The aeroelastic response of the composite plate is analysed using the DLM [32], a computational aerodynamic model widely employed in the study of unsteady aerodynamic flows. DLM is particularly adept at handling problems related to subsonic and supersonic flows around complex configurations. By discretising the surface of the structure into a lattice of doublet panels, DLM approximates the potential flow field, enabling the efficient calculation of aerodynamic pressure distributions.

This method is important for the understanding the interaction between aerodynamic forces and structural deformations, a critical aspect in predicting aeroelastic phenomena such as flutter and response to gusts. The main aeroelastic phenomena studied within this case are now presented.

2.1. Aeroelastic response

Aeroelasticity plays a pivotal role in the structural integrity and performance of aircraft components subjected to aerodynamic forces. This study advances the understanding of aeroelastic behaviour by considering a composite wing structure, represented through a simplified plate model. The aerodynamic load prediction employs the DLM, leveraging the capabilities of the *MSC NASTRAN* software for comprehensive aeroelastic analysis.

2.1.1. Static aeroelastic analysis

The first step in aeroelastic assessment involves evaluating the static integrity of the composite structure, which is the ability of the plate to sustain and revert to its initial configuration under standard operational load conditions. The equilibrium between aerodynamic and structural forces is the basis of static aeroelastic stability [2], captured by the equation:

$$\mathbf{Kq} = \mathbf{F}_a(\mathbf{q}; \rho, U), \tag{2}$$

where $\mathbf{K}$ is the stiffness matrix that characterises the rigidity of the plate, $\mathbf{q}$ denotes the generalised displacement vector, and $\mathbf{F}_a$ symbolises the aerodynamic force vector, which is a function of the wing deformed geometry and prevailing flight conditions, defined by air density (ρ) and flight speed (U).

2.1.2. Flutter analysis

Flutter is a destructive instability that can result from the interaction of aerodynamic, elastic and inertial forces. It is critical to predict and mitigate this phenomenon to ensure flight safety. The investigation into flutter involves calculating the aeroelastic stability of the fluid–structure coupled system and identifying the flutter boundary, which is demarcated by the critical flutter speed. The governing equation for flutter analysis in the time domain is as follows:

$$\mathbf{M}\ddot{\mathbf{q}} + \mathbf{Kq} = \mathbf{F}_a(\mathbf{q}, \dot{\mathbf{q}}; \rho, U), \tag{3}$$

where $\mathbf{M}$ is the mass matrice of the structural system.

Transitioning to the frequency domain for detailed flutter analysis, the aeroelastic equations transform to:

$$(\mathbf{K} + \rho U^2 \mathbf{K}_a(\omega) - \lambda^2 \mathbf{M})\hat{\mathbf{q}} + i\lambda\rho U \mathbf{C}_a(\omega)\hat{\mathbf{q}} = \mathbf{0}, \tag{4}$$

and

$$\lambda = \sigma + i\omega, \tag{5}$$

with λ representing the complex eigenvalue of the system, consisting of the growth rate (σ) and frequency (ω), $\mathbf{K}_a$ and $\mathbf{C}_a$ indicating aerodynamic stiffness and damping matrices, and $\hat{\mathbf{q}}$ denoting the mode shapes amplitude [33].

2.1.3. Wind gust response analysis

The structural response to transient wind gusts is primordial to aeroelastic studies as shown in the works [27,30], as gust loads can induce immediate and potentially severe stress on the aircraft structure. The dynamic response of the composite plate to gusts is characterised by transient analysis, which accounts for the time-dependent nature of the unsteady aerodynamic forces:

$$\mathbf{M}\ddot{\mathbf{q}} + \mathbf{C}\dot{\mathbf{q}} + \mathbf{Kq} = \mathbf{F}_a(\mathbf{q}; \rho, U) + \mathbf{F}_{gust}(t), \tag{6}$$

where $\mathbf{F}_{gust}(t)$ denotes the time-varying force vector due to gust impact, which is superimposed on the steady aerodynamic forces $\mathbf{F}_a$. The gust loading is typically modelled as a step function or a more complex function representing the gust profile affecting the aircraft velocity field.

The approach outlined here integrates static and dynamic aeroelastic analyses to provide a thorough evaluation of the composite structure's performance under varied flight scenarios. Ensuring static stability under standard conditions, quantifying the critical flutter speed, and evaluating the gust response are essential components of the design process, contributing to the resilience and reliability of the composite wing structure.

2.2. Composite material multi-scale approach

The optimisation process is centred around the search for the optimum stacking sequence, defined as a series of ply angles θ_{opt}. However, the stacking sequence design space presents certain challenges. Notably, the degrees of freedom within this design space are not constant, as they depend on the number of plies, which is one of the optimisation parameters. Additionally, this design space exhibits numerous local minima, complicating the task of finding the globally optimal solution. Moreover, the angles are usually not part of a continuous space and are set as a list of discrete values $(0°, \pm15°, \pm30°, \pm45°, \pm60°, \pm75°, 90°)$, to take into account manufacturing constraints [34]. Furthermore, the mechanical response to variations in the stacking sequence is notably irregular, which complicates the creation of a surrogate model capable of accurately replicating these responses. To address these complexities, we introduce a multi-scale technique where the mesoscale (stacking sequence) is transformed via homogenisation to the macroscale (lamination parameters). This transformation simplifies the entry variables for the surrogates and reduces the complexity of the mechanical response predicted by the surrogate models.

2.2.1. Composite material homogenisation

Beginning with the classical laminate plate theory [7], we can define the behaviour of composite materials using the matrices A, B, and D. Matrix A pertains to membrane rigidity, while matrix D corresponds to flexure rigidity. Notably, matrix B captures the complex interplay of Membrane/Bending/Torsion coupling inherent in the composite structure. Concurrently, vectors $\mathbf{N}$ and $\mathbf{M}$ denote the resultant stress and moment to which the plate is exposed, giving rise to strain (ϵ) and curvature (κ).

Considering the matrices A, B, and D, the behaviour of a composite stack is characterised by a total of 18 variables. These variables are contingent on both the stacking sequence and the material properties. As all these variables are contingent on material properties, optimising them becomes challenging, particularly when the material properties are held constant.

At this point, we explore the lamination parameter design approach, which aims to decouple the geometric factors from the mechanical properties of the material considered. Considering θ as the orientation of different plies, t as the total thickness of the composite, and ζ as the through-thickness coordinate, the definition of the lamination parameters (LPs) is as follows:

$$\begin{aligned}
\mathbf{v}^{\mathbf{A}}_{[\mathbf{1},\mathbf{2},\mathbf{3},\mathbf{4}]} &= \frac{1}{t}\sum_{k}^{N} z_k - z_{k-1}\left[\cos(2\theta_k), \sin(2\theta_k), \cos(4\theta_k), \sin(4\theta_k)\right], \\
\mathbf{v}^{\mathbf{B}}_{[\mathbf{1},\mathbf{2},\mathbf{3},\mathbf{4}]} &= \frac{4}{t^2}\sum_{k}^{N} \frac{z_k^2 - z_{k-1}^2}{2}\left[\cos(2\theta_k), \sin(2\theta_k), \cos(4\theta_k), \sin(4\theta_k)\right], \\
\mathbf{v}^{\mathbf{D}}_{[\mathbf{1},\mathbf{2},\mathbf{3},\mathbf{4}]} &= \frac{12}{t^3}\sum_{k}^{N} \frac{z_k^3 - z_{k-1}^3}{3}\left[\cos(2\theta_k), \sin(2\theta_k), \cos(4\theta_k), \sin(4\theta_k)\right].
\end{aligned} \tag{7}$$

After establishing the LPs, the total number of unknowns for the optimisation problem concerning the composite stack is reduced to 12 LPs and 5 fixed material invariants, determined by the mechanical properties of the material. Subsequently, by employing the LPs and material invariants, we can compute the matrices A, B, and D as described in the works of Tsai et al. [7],

$$\mathbf{A} = t\,\tilde{\mathbf{A}}\left(\mathbf{v}^{\mathbf{A}}\right), \quad \mathbf{B} = \frac{t^2}{4}\tilde{\mathbf{B}}\left(\mathbf{v}^{\mathbf{B}}\right), \quad \text{and} \quad \mathbf{D} = \frac{t^3}{12}\tilde{\mathbf{D}}\left(\mathbf{v}^{\mathbf{D}}\right). \tag{8}$$

The 12 LPs describing the composite behaviour will be denoted as $\mathbf{v}$. These parameters, together with the material properties of the laminate, represent the composite's A, B, and D matrices. In the context of our study, the number of plies, N, also plays a crucial role in the final outcome, thus extending our homogenised design space to 13 variables in the form of $(\mathbf{v}, N)$.

However, the specific case of the aeroelastic plate under investigation is one of pure bending, which allows us to focus solely on the D matrix. For simplicity's sake, we have imposed a design condition on the composite plies which simplifies the problem allowing us to only consider $\mathbf{v}_1^D$ and $\mathbf{v}_3^D$ within the LPs, simplifying our homogenised space even further. Therefore, in order to sum up the homogenisation process, the result is the transformation of the detailed stacking sequence $\boldsymbol{\theta}$ into a more manageable form by representing it as a set of three homogenised variables, $(\mathbf{v}_1^D, \mathbf{v}_3^D, N)$.

2.3. Maximum strain constraint

Incorporating strength constraints into the lamination parameter optimisation process for composite laminates, typically defined at the ply scale, presents unique challenges. Drawing upon the work of [35–37], we leverage conservative first-ply failure envelopes based on failure criteria such as Tsaï-Wu and the modified Tsaï-Hill. These envelopes are defined in terms of macroscopic in-plane strains and are independent of ply angle, facilitating their application to a homogenised laminate description.

A new approach proposed by [10] involves sampling ply orientations to compute in-plane failure envelopes, with the conservative failure envelope emerging as the intersection of all individual safe regions. This aggregate envelope can be efficiently approximated by an ellipsoid, characterised by a matrix $\boldsymbol{\Phi}$ and centre c, and incorporated into the optimisation as a constraint:

$$(\epsilon - \mathbf{c})^T \boldsymbol{\Phi} (\epsilon - \mathbf{c}) \leq 1 \tag{9}$$

where ϵ denotes the macroscopic strains. This method accounts for structural bending by evaluating failure criteria at the laminate's outer surfaces.

The strain constraint imposed throughout this work will utilise a conservative failure envelope based on the modified Tsaï-Hill criterion, expressed for ply-scale stresses as:

$$\left(\frac{\sigma_{11}}{X^*}\right)^2 - \frac{\sigma_{11}\sigma_{22}}{X_t X_c} + \left(\frac{\sigma_{22}}{Y^*}\right)^2 + \left(\frac{\tau_{12}}{S^*}\right)^2 \leq 1, \tag{10}$$

where X^* and Y^* represent tensile or compressive strengths based on stress sign, and S^* is the shear strength. The conservative envelopes for both Tsaï-Wu and modified Tsaï-Hill criteria, alongside their ellipsoidal approximations, highlight the optimisation's strength constraint definition.

2.4. Formulation of the probabilistic optimisation problem

Our objective in the optimisation of composite wing structures is to minimise the expected gust response while also minimising overall mass, all of this under uncertainties in the composite ply fabrication. The optimisation accounts for variations in manufacturing imperfections that affect the aeroelastic response and structural integrity.

Objective Function: The goal is to find the stacking sequence $\bar{\boldsymbol{\theta}} = [\bar{\theta}_1, \bar{\theta}_2, \ldots, \bar{\theta}_N]$ which minimises the expected value of the gust-induced maximum bending moment, denoted by M_x, together with the number of plies N, representing the material usage and proportional to the weight. The optimisation function under a probabilistic framework is expressed as:

$$\mathbb{E}[f(\boldsymbol{\theta})] = N + w_{\text{gust}} \cdot \mathbb{E}[M_x(\boldsymbol{\theta})], \tag{11}$$

where $\mathbb{E}[\cdot]$ denotes the expected value operator, indicating that our optimisation considers the average performance over the variability in the input ply angles $\boldsymbol{\theta} \sim \mathcal{N}(\bar{\theta}, \sum)$ and N corresponding to the dimension of $(\boldsymbol{\theta})$. The coefficient w_{gust} is a weighting factor that scales the impact of the gust effect.

Constraints: The design is subjected to probabilistic constraints, ensuring that the likelihood of exceeding critical performance thresholds remains within acceptable bounds:

1. **Flutter Speed Constraint:** The probability of the flutter speed falling below a critical value should be minimised to ensure aeroelastic stability:

$$\mathbb{P}(V_{\text{flutter}}(\boldsymbol{\theta}) < V_{\min}) \leq \mathbb{P}^V_{\text{limit}}, \tag{12}$$

2. **Maximum Equivalent Strain Constraint:** The probability of the equivalent strain surpassing a maximum allowable level must be controlled to avoid structural failure:

$$\mathbb{P}(\epsilon_{\text{equivalent}}(\boldsymbol{\theta}) > \epsilon_{\max}) \leq \mathbb{P}^\epsilon_{\text{limit}}, \tag{13}$$

In these expressions, $\mathbb{P}(\cdot)$ represents the probability of the event occurring, which should be kept below the limit $\mathbb{P}_{\text{limit}}$, defined based on safety and performance requirements.

Probabilistic Optimisation Problem: The reformulated optimisation problem, now cast in a probabilistic setting, aims to find a design that minimises the expected objective function while satisfying the constraints with high confidence:

$$\begin{aligned} \underset{(\bar{\theta})}{\text{minimise}} \quad & \mathbb{E}[f(\boldsymbol{\theta})] \\ \text{subject to} \quad & \mathbb{P}(V_{\text{flutter}}(\boldsymbol{\theta}) < V_{\min}) \leq \mathbb{P}^V_{\text{limit}}, \\ & \mathbb{P}(\epsilon_{\text{equivalent}}(\boldsymbol{\theta}) > \epsilon_{\max}) \leq \mathbb{P}^\epsilon_{\text{limit}}. \end{aligned} \tag{14}$$

The optimisation formulation leverages the statistical characterisation of uncertainties to deliver a stacking sequence that ensures performance robustness and maintains structural safety under probabilistic material behaviour considerations.

3. Methodology

The methodology proposed within this work consists of a two-step process comparable to the works proposed on [23]. The first step proposes a Surrogate Model Based Design Optimisation (SMBDO), as described in [38], which involves the construction of surrogate models within a deterministic framework and an iterative algorithm to ameliorate said models. The second step utilises these models for RBDO. This methodology will help in dealing with the multi-scale nature of the original design spaces, where the stacking sequence of angles $\boldsymbol{\theta}$ represents a non-convex design space with many local minima, and the LPs (v, N) represent the continuous and convex transformed space.

Within this study, a different surrogate model will be created for each aeroelastic response (static, gust and flutter) with three design variables $(\mathbf{v}_1^D, \mathbf{v}_3^D, N)$, the two LPs being continuous and the number of plies being a discrete variable. The initial surrogate models are created as KRG surrogate models which are chosen for their precision in prediction and ability to provide uncertainty estimates, making them ideal for optimising complex systems where direct sampling is expensive. The KRG surrogate models are created using the SMT library [39] which allows for a straightforward Python environment and permits the mixed use of discrete and continuous variables. The KRG surrogate models are optimised via an EGO approach [22], which facilitates the efficient exploration of the design space. All of the EGO process will be conducted within a deterministic framework simplifying the previously presented formulation of the optimisation problem.

The RBDO phase introduces variability in the angles, representing the uncertainties in manufacturing and material properties, and uses GAs to find the optimum stacking sequences. Each evaluation of the fitness of the stacking sequences proposed throughout the evolutionary algorithm execution will make use of the surrogate models created previously within the first step. The fitness will be the evaluation of the reliability-based optimisation problem presented previously.

3.1. Surrogate model refinement

The implementation of EGO in this study is tailored to operate within the homogenised design space defined by the LPs ($\mathbf{v}$) and the number of plies N. This space is a transformation of the original, highly non-convex stacking sequence problem into a convex, semi-continuous domain that is amenable to gradient-based optimisation techniques. Moreover, by adopting this homogenisation approach, we effectively reduce the complexity inherent to the discrete nature of the stacking sequences design space and the non-constant number of inputs, facilitating a more efficient and cheaper generation of surrogate models.

EGO is a sequential approach for global optimisation problems, particularly useful when dealing with expensive objective function evaluations. In this first step of the proposed methodology a simplification of the probabilistic problem's constraints is introduced. Specifically, we convert the probabilistic constraint, originally formulated as shown in Eqs. (12) and (13), into a deterministic constraint. This modification entails replacing the probabilistic condition with a deterministic equivalent, thereby reducing the computational complexity and facilitating a more straightforward optimisation process.

$$\begin{aligned} \underset{(\mathbf{v},\boldsymbol{N})}{\text{minimise}} \quad & f(\mathbf{v},\boldsymbol{N}) \\ \text{subject to} \quad & V_{\text{flutter}}(\mathbf{v},\boldsymbol{N}) < V_{\min}, \\ & \epsilon_{\text{equivalent}}(\mathbf{v},\boldsymbol{N}) > \epsilon_{\max} \end{aligned} \tag{15}$$

3.1.1. Efficient global optimisation

In the development of an EGO strategy, the selection of an appropriate initial Design of Experiments (DOE) is critical for ensuring a comprehensive initial exploration of the design space. Latin Hypercube Sampling (LHS) [40] is chosen for this purpose due to its superior efficiency and coverage compared to traditional random sampling methods. LHS ensures that the entire range of each design variable is explored by dividing it into intervals of equal probability. This method guarantees that each interval is sampled only once, thereby minimising the risk of clustering and maximising the diversity of the sample points. Consequently, LHS provides a more uniform spread of initial points in the design space, which is particularly advantageous for constructing KRG surrogate models. By facilitating a better initial approximation of the objective function landscape, LHS enhances the efficiency of the optimisation process, leading to more reliable and robust design solutions in the context of composite materials optimisation under aeroelastic constraints.

The initial points defined by the LHS method are evaluated in the objective and constraint functions to establish a performance baseline. This initial evaluation is critical as it grounds the surrogate models in actual observed data, providing a reliable starting point for the optimisation process.

The KRG surrogate models, which are Gaussian Processes (GPs), use this data to predict the behaviour of the objective function and constraints. Functions that are approximated using a surrogate model are indicated with a hat symbol. This notation is consistently used to differentiate between the original functions and their surrogate model approximations.

The EGO algorithm iteratively adds points to these models by optimising an acquisition function, which is key to identifying new, informative data points. This process is crucial for refining the surrogate model's predictions over successive iterations. The surrogate models are dynamically updated as new data points are incorporated, this continuous integration of new data points leads to a progressive improvement in the model's accuracy. The core of this iterative process lies in the optimisation of an acquisition function, known as Expected Improvement Constrained Optimisation ($EICO$) [25]. The EICO infill function is initially solved using a differential evolution [41] technique to broadly scan the design space. Following this, an L-BFGS-B optimiser fine-tunes the solution, pinpointing the optimum of the infill function. This hybrid approach to solving mixed functions can be found in the works of [42,43]. This two-step optimisation approach, starting with differential evolution for a global search followed by refinement using L-BFGS-B, ensures a comprehensive exploration of the design space within the infill function optimisation. This methodology used for solving the optimisation of the infill function can be compared to the classical approach of AK-MCS [44]. This optimisation has been adapted to solve the optimisation of the $EICO$ function within a non-continuous design space such as the one defined within the modified KRG surrogate models used. Once the EGO iterative methodology is defined, we now proceed to introduce the constrained EGO acquisition function.

3.1.2. Expected improvement

The standard form of EI [22] is defined as the expected increase in objective function value over the current best observation $f(\mathbf{v}^*, N^*)$, and is given by:

$$EI(\mathbf{v}, N) = \mathbb{E}[\max(\hat{f}(\mathbf{v}^*, N^*) - \hat{f}(\mathbf{v}, N), 0)]. \tag{16}$$

Assuming a Gaussian Process model for the objective function with mean $\mu(\mathbf{v}, N)$ and standard deviation $\sigma(\mathbf{v}, N)$, the EI at any point $(\mathbf{v}, N)$ in the design space can be expanded using the properties of the normal distribution as follows:

$$\begin{aligned} EI(\mathbf{v}, N) =& (\hat{f}(\mathbf{v}^*, N^*) - \mu(\mathbf{v}, N))\Phi(Z(\mathbf{v}, N)) \\ &+ \sigma(\mathbf{v}, N)\phi(Z(\mathbf{v}, N)), \end{aligned} \tag{17}$$

where $Z(\mathbf{v}, N)$ is the improvement potential standardised,

$$Z(\mathbf{v}, N) = \frac{\hat{f}(\mathbf{v}^*, N^*) - \mu(\hat{f}(\mathbf{v}, N))}{\sigma(\hat{f}(\mathbf{v}, N))}, \tag{18}$$

and Φ and ϕ are the cumulative and probability density functions of the standard normal distribution, respectively.

3.1.3. Probability of feasibility

In order to consider the constraints within the acquisition functions of the EGO algorithm, the probability of feasibility (PoF) is introduced [45]. The probability of feasibility for each constraint, modelled separately by individual Gaussian Processes, estimates how likely a point is to respect the constraint of the optimisation problem taking into account the variability of the surrogate model. The PoF can be calculated as follows:

$$PoF(\mathbf{v}, N) = \prod_{i=1}^{m} \Phi\left(\frac{-\mu_{\text{con}_i}(\hat{g}(\mathbf{v}, N))}{\sigma_{\text{con}_i}(\hat{g}(\mathbf{v}, N))}\right), \tag{19}$$

3.1.4. Expected improvement in constrained optimisation

The EGO algorithm iterates by selecting the point $(\mathbf{v}_{\text{next}}, N_{\text{next}})$ that maximises the Expected Improvement multiplied by the Probability of Feasibility, which incorporates both the desire for improvement and the need to satisfy constraints [46]:

$$(\mathbf{v}_{\text{next}}, N_{\text{next}}) = \arg\max_{(\mathbf{v},N)} (EI(\mathbf{v}, N) \times PoF(\mathbf{v}, N)). \tag{20}$$

Having established a refined approach to surrogate model optimisation through EGO, we now transition to the next step: RBDO. This shift represents a move from the theoretical and procedural enhancement of models to their practical application in addressing variability and uncertainties in composite structures.

3.2. Reliability-based design optimisation with genetic algorithms

The RBDO process is initiated in a design space defined by a constant number of plies. This number is determined based on the ply count of the deterministic solution obtained from the previous optimisation stages N_{opt}. If the RBDO process within this fixed ply count does not yield a viable solution, the optimisation is then extended to the space of $N_{opt} + 1$ plies. The RBDO is solved via a GA given that this approach ensures a simplified exploration of the stacking sequence

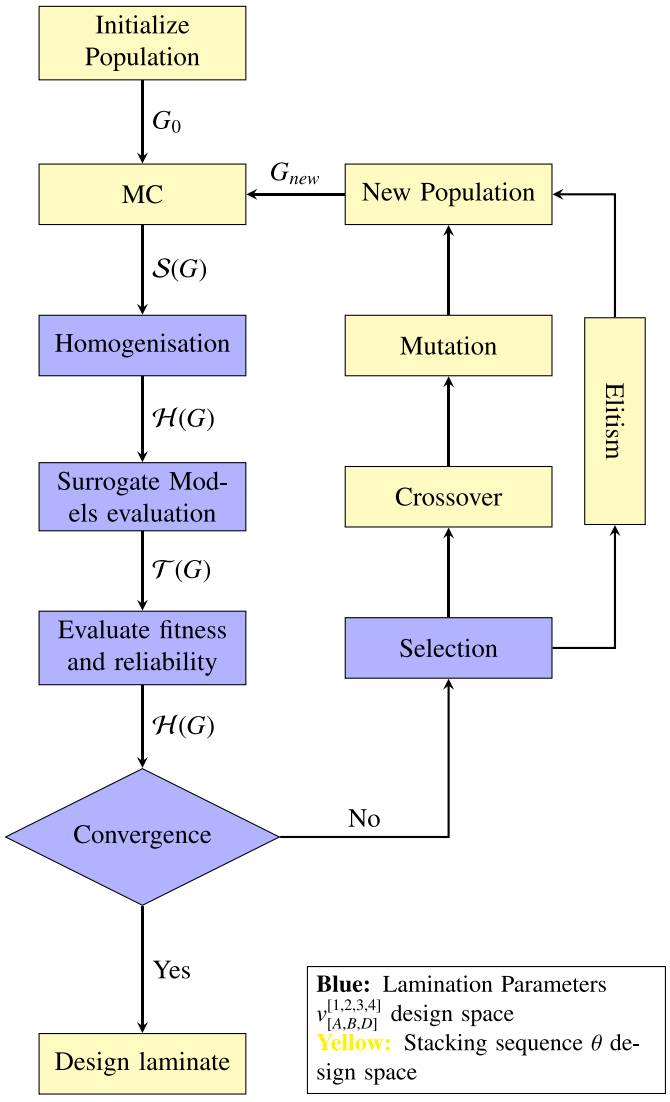

Fig. 2. Flowchart of the standard Genetic Algorithm process including the generation of stacking sequences using Monte Carlo (MC) simulation and homogenisation of θ.

design space. The key challenge addressed is the inherent variability in material properties and manufacturing processes, which is represented by introducing a statistical error into the angle of each ply as mentioned in Section 2.

The proposed workflow for the GA is shown in Fig. 2. This visualisation serves as a comprehensive guide to the sequential steps and processes integral to our GA's operation. In the following section, we will examine each component within the workflow. The step-by-step breakdown will provide insight into the algorithm's structure, from the initialisation of the population to the final evaluation stages, highlighting the role of processes such as MC sampling, homogenisation and surrogate model evaluation.

1. **Initial Population Generation:** The GA begins by generating a random initial population of stacking sequences $G = \{\theta_1, \theta_2, \dots, \theta_N\}$. This initial step ensures a diverse foundation for the evolutionary optimisation process and the size of this population will determine the initial exploration of the design space.
2. **MC Sampling:** Upon establishing a population G, a MC analysis is conducted for each individual θ_n. For an individual θ_i, we perform M MC simulations, yielding a set of outcomes $S(\theta_i) = \{s_{i1}, s_{i2}, \dots, s_{iM}\}$. We can also define the overall computation of the MC sampling of the entire generation as $\mathcal{S}(G) = \{S(\theta_1), S(\theta_2), \dots, S(\theta_N)\}$
3. **Homogenisation $\theta \rightarrow v$:** Being each outcome s_{ij} from the MC sampling an individual stacking sequence θ, each s_{ij} undergoes the homogenisation process in order to transform the θ values into v, by using the homogenisation techniques presented earlier. This homogenisation step will facilitate the use of the surrogate models previously computed for the objective function and constraints as the surrogate models are functions defined as $\hat{f}(v, N)$. The output from the homogenisation problem can be noted as (v_{i1}, N_{i1}) for each MC sample, $H(\theta_i) = \{(v_{i1}, N_{i1}), (v_{i2}, N_{i2}), \dots, (v_{iM}, N_{iM})\}$ and $\mathcal{H}(G) = \{H(\theta_1), H(\theta_2), \dots, H(\theta_N)\}$ for the entire generation.
4. **Surrogate Model evaluations:** The homogenised outcomes are now evaluated through the different surrogate models. Those models assess each individual's performance with respect to our aeroelastic criteria: static maximum equivalent strain, flutter speed, and gust response. The surrogate model offers a computationally efficient mechanism to approximate these responses, enabling rapid evaluation of the extensive number of individuals and scenarios generated through the MC simulations. The output of this block can be denoted as $\mathcal{T}(G) = \{T(\theta_1), T(\theta_2), \dots, T(\theta_N)\}$ for the entire generation and $T(\theta_i) = \{t_{i1}, t_{i2}, \dots, t_{iM}\}$ for each of the individuals containing the aeroelastic response of each ply generated during the MC sampling.
5. **Fitness and reliability computation:** The results obtained from the Surrogate Model evaluation of all the MC samples, $\mathcal{T}(G)$, are now used to compute the fitness and failure probability of each of the individuals. For the fitness function, we can recall function (11), where the MC sampling will allow for a computation of $\mathbb{E}[f(\theta)]$. Moreover, using a modified MC algorithm which is described later in this chapter, we can also compute the values of $\mathbb{P}(V_{\text{flutter}}(\theta) < V_{\min})$ and $\mathbb{P}(\epsilon_{\text{equivalent}}(\theta) > \epsilon_{\max})$ taking into account the variability of our constraints surrogate models. This part of the algorithm can be denoted as $\mathcal{F}(G) = \{F(\theta_1), F(\theta_2), \dots, F(\theta_N)\}$ and it will give for each individual as:

$$F(\theta_i) = (\mathbb{E}[f(\theta_i)], \mathbb{P}(\epsilon_{\text{equivalent}}(\theta_i) > \epsilon_{\max}), \mathbb{P}(V_{\text{flutter}}(\theta_i) < V_{\min})) \tag{21}$$

6. **Ranking and selection:** This step involves ranking the individuals from the current generation to be the parents of the next generation. Within the developed GA algorithm the individuals are first classed into three subgroups:

   - Group one contains the individuals who satisfy both constraints, defined in Eqs. (12) and (13). Ranking within this group is based solely on fitness function defined in Eq. (11). With fitter individuals having a higher probability of being chosen. This process ensures that traits from the best performers are passed on to the new Generations.
   - Group two contains the individuals who only satisfy one of the imposed constraints. Within this group we class the individuals by the average value of the violated constraint and rank them from highest to lowest in the case of the strain constraint and lowest to highest for the flutter constraint.
   - Group three contains the individuals who do not satisfy any of the constraints. Those are ranked randomly and are the most likely to not be included in the next generation

   The lists of ranked individuals are now joined so that group one is the highest class and group three is the lowest. A certain percentage of the top of this list of individuals is now taken and used within the next steps.

7. **Elitism:** Elitism is a strategy where the best performing individuals from the current generation, quantified by their fitness F_i, are automatically passed to the next generation. This ensures that the GA does not lose the best solutions found so far, maintaining and potentially improving the overall quality of the population. Specifically, E_n top-performing individuals are preserved, fostering the retention of advantageous genetic information.
8. **Crossover and Mutation:** During crossover, pairs of parent individuals are combined to form offspring for the next generation, with a crossover rate of C_r. This step simulates genetic recombination, creating diversity within the population. Mutation introduces random changes to the offspring's traits at a mutation rate of M_r, mimicking natural genetic mutations. This step is crucial for maintaining genetic diversity within the population, allowing the algorithm to explore a wider search space and potentially find better solutions by escaping local optima. The crossover and mutation techniques used in this work are based on the works of [4,47].
9. **New population:** The new generation is formed by selecting the next generation's individuals through the processes of selection, elitism, crossover, and mutation. This new population, consisting of N individuals, then undergoes the entire process described, going through the MC sampling, the homogenisation, surrogate model evaluation, and fitness/reliability computation. Each step is designed to refine and evaluate the population based on specific performance criteria, ensuring that each new generation G_{max} progressively moves towards optimal solutions.
10. **Convergence:** The algorithm is considered to converge when there is no significant improvement in the population's fitness over a set number of generations, or when it reaches the predefined maximum number of generations, G_{max}. Convergence indicates that the GA has potentially found an optimal or near-optimal solution within the search space. The fitness threshold for convergence and the criteria for significant improvement are defined based on the specific objectives and constraints of the problem at hand.

This methodological framework, from initial population generation to detailed surrogate model evaluation, encapsulates the essence of our GA approach. By integrating stochastic analysis with advanced homogenisation techniques and surrogate modelling, we robustly identify optimal stacking sequences that fulfil or surpass our performance and reliability criteria under uncertain conditions.

The optimisation process continues through these steps, iteratively refining the population until a convergence criterion is met. This criterion signifies the attainment of an optimal stacking sequence that balances the objective function's requirements with the reliability constraints, achieving a robust and high-performance design.

3.2.1. Modified Monte Carlo analysis

The MC simulation used to compute the probability of failure of the composite structure is modified to also incorporate the probability of feasibility of the surrogate model's predictive uncertainty [48]. This way it is assured that the final failure probability also accounts for the predictability errors of the surrogate model. For each sampled design, the probability that the design satisfies the constraints is calculated and used as a continuous measure within the MC simulation:

$$\mathbb{P}_f(\mathbf{v}, N) = 1 - \sum_{i=1}^{m} \Pi_i(\mathbf{v}_i, N) PoF_i(\mathbf{v}_i, N) \tag{22}$$

where Π_i is the binary indicator function of the constraint violation, PoF_i is the probability of feasibility (Eq. (19)) for the ith constraint, $\mathbf{v}_i$ is the vector of LPs of one sample, and N the number of plies.

The optimisation process iterates through genetic operations, selection, crossover, and mutation, to evolve the population towards sequences with better fitness values. The RBDO loop concludes when a pre-defined convergence criterion is satisfied, signifying the attainment of an optimal design with the desired reliability and performance characteristics.

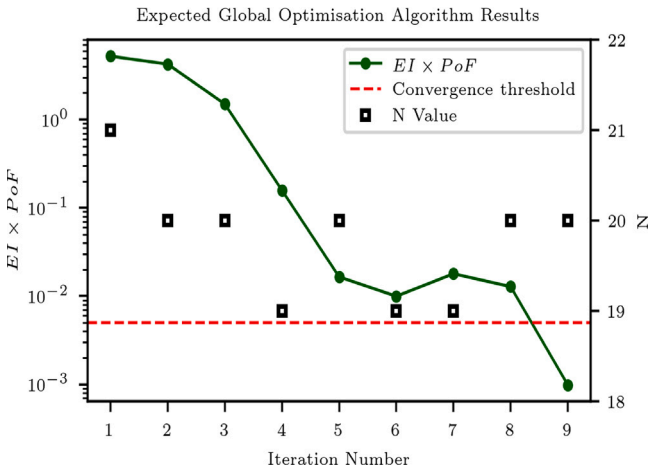

Fig. 3. Convergence plot of the EGO process (blue dots) and N value of the newly computed points (green squares). The red dashed line indicates the stopping criteria for the EGO.

4. Results

The results, derived from applying the methodology described in Section 3 to the aeroelastic challenge outlined in Section 2, are now presented. This segment highlights the effectiveness of our approach, combining EGO and GAs to optimise composite plates under aeroelastic constraints. Our findings demonstrate significant improvements in both material reliability and aeroelastic performance, showcasing the potential of the proposed optimisation framework in composite design. The results obtained from the surrogate model construction have been validated and compared with other surrogate model construction approaches found in the literature. Moreover, the final GA results have also been validated at both a quality level and a computational cost level.

4.1. Adaptive construction of the surrogate models for the aeroelastic responses

EGO process is employed to develop surrogate models for the objective function (gust response) and for the constraints (equivalent strain and the limit flutter speed), those KRG surrogate models depending on the continuous variables $\mathbf{v}_1^D$, $\mathbf{v}_3^D$, and the discrete variable N. The process involves an interplay of exploring and exploiting the design space to form a reliable and accurate model. For this particular study case, we have set the limit flutter speed at $V_{\text{min}} = 175.1$ m/s and the limit equivalent strain at $\epsilon_{\text{max}} = 1.6 \times 10^{-3}$.

The EGO process starts with the initial DoE, setting the stage for subsequent exploration. The scatter plot shown in Fig. 4 illustrates with circles the starting points in the LPs design space spanned by $\mathbf{v}_1^D$, $\mathbf{v}_3^D$, and N. For the initial phase of this study, the DoE was strategically established with 20 initial design points, leveraging the LHS method for their distribution. This approach facilitated the exploration of the design variables $\mathbf{v}_1^D$ and $\mathbf{v}_3^D$ as continuous factors within the range of -1 to 1, while the variable N was treated as a discrete factor, varying between 10 and 30.

To evaluate the efficiency and effectiveness of the proposed EGO process, the convergence plot is examined. The convergence plot, Fig. 3, illustrates the trajectory of the optimisation process across iterations. This plot remarks the model's ability to refine its predictions and approach an optimal solution iteratively. The reduction in the objective function's value is indicative of the model's maturing understanding of the underlying physical phenomena. In the evolution of the EGO algorithm's convergence, an unexpected increment in the $EI \times PoF$ metric is observed at iteration 7, subsequent to the addition of the design point

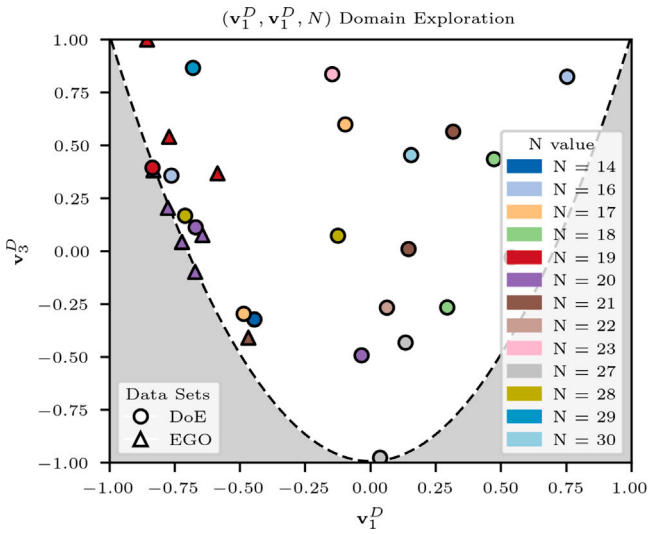

Fig. 4. DoE scatter plot showing the simulations added throughout the EGO process in the $(\mathbf{v}_1^D, \mathbf{v}_3^D)$ space (top view with N-axis perpendicular to the view plane).

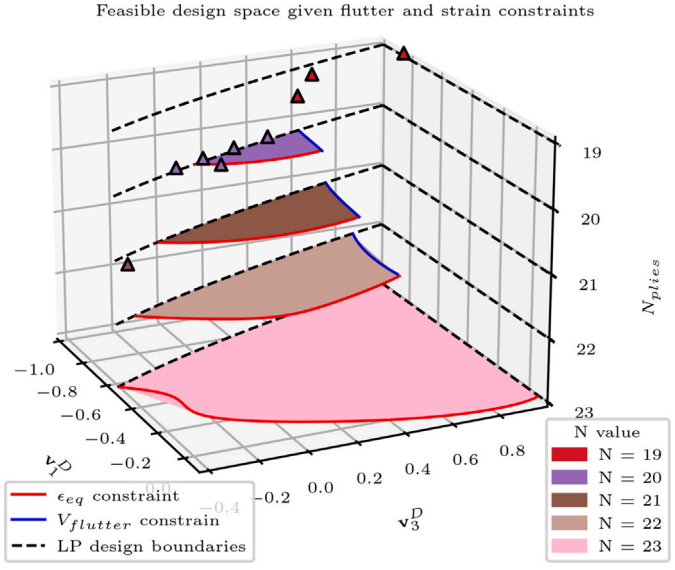

Fig. 5. Sliced 3D plot showing the feasible design regions when the constrains are imposed within the design space, together with the points computed via the Efficient Global Optimisation.

at iteration 6. This anomaly can be attributed to the newly added point exhibiting significantly low variability, which inadvertently introduces a minor distortion in the surrogate model due to an ill-conditioning of the KRG surrogate model [49]. However, this perturbation is transient and is systematically rectified in the ensuing iteration, reinstating the surrogate model's fidelity and continuing the convergence process. This incident underscores the dynamic adaptability of the EGO framework in responding to and correcting for deviations in the surrogate model, ensuring robust optimisation progress.

Fig. 4 illustrates the final points computed throughout the design space, with triangle shapes, and the initial DoE with circles. The gradual addition of points reflects the EGO's ability to navigate and sample the design space, seeking regions of high potential based on the current understanding and definition of the model. It is worth remarking how most of the points have been added at $N = 20$ indicating that the EGO algorithm has efficiently explored the design space and has finally converged at a number of plies. Furthermore, the Probability

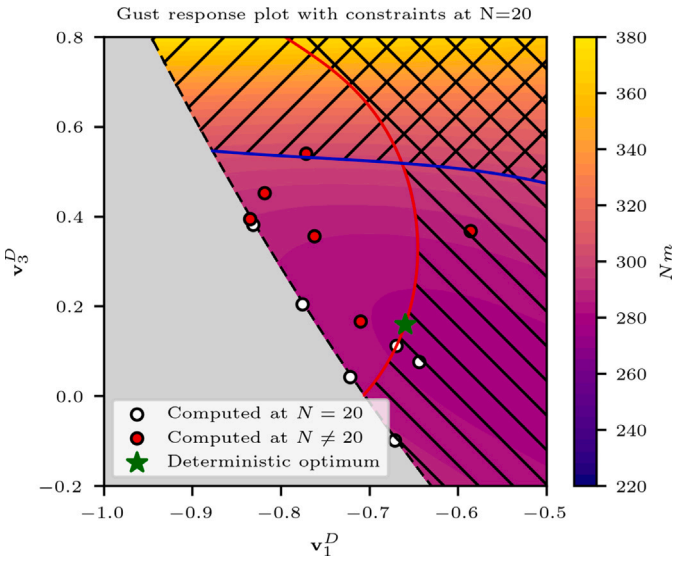

Fig. 6. Isocontours of the gust response showing all used computed simulations projected onto the N = 20 ply space. Constraints are also indicated (black for flutter and red for strain).

of Feasibility factor has been also important, given that the algorithm has clearly explored non-feasible solutions such as the point at $N = 14$. This exploration of both feasible and non-feasible regions contributes to a more comprehensive understanding of the design space, ensuring that the final solution is not only optimal but also robust against the existence of local minima.

Fig. 5 depicts the feasible design surfaces at different N values for the surrogate models. These areas are delimited by the strain and flutter constraints, shown in red and blue, together with the LP design limits [7]. We can observe that the first area appears at $N = 20$, therefore indicating the value of our $N_{opt} = 20$. Along with the 3D slices, we plot the points computed via the EGO process to show the areas that have been more thoroughly explored. The 3D visualisation of this plot allows for the observation of the overall feasible regions of the surrogate models in the $(\mathbf{v}_1^D, \mathbf{v}_3^D, N)$ design space. However, the higher concentration of points at $N = 20$, also depicted in Figs. 3 and 4, leads to a better approximation of the real response on this design surface. Outside the region with concentrated points, the predictions might be poorer due to less information availability in the surrogate model training process. However, these region are not meant to be explored during the following RBDO step.

The analysis then narrows its focus to a specific number of plies $N = 20$, which, as previously explained, is a region particularly favoured by the EGO process. The concentration of study points at this number of plies suggests a higher level of confidence in the model's predictions. Given that the objective function actively attempted to reduce the number of plies, and the first feasible configuration is at $N = 20$, the deterministic optimum can be easily found by fixing the N variable and using a $SLSQP$ [50] optimiser for the $(\mathbf{v}_1^D, \mathbf{v}_3^D)$ variables. The deterministic optimum found is indicated in Fig. 6 with a green star.

Within Fig. 6, the points computed specifically at $N = 20$ are distinguished in white, illustrating their direct relevance to this layer. In contrast, points calculated at other ply counts, which provide valuable insights for the surrogate model's accuracy, are projected onto this plane and are represented in red. This colour coding not only helps for visual differentiation but it also emphasises the influence of points computed at $N \neq 20$ on enhancing the precision of the surrogate model at $N = 20$.

Fig. 7, shows the evolution of the PoF metric around the constraints. With green showing the feasible regions and red showing the regions

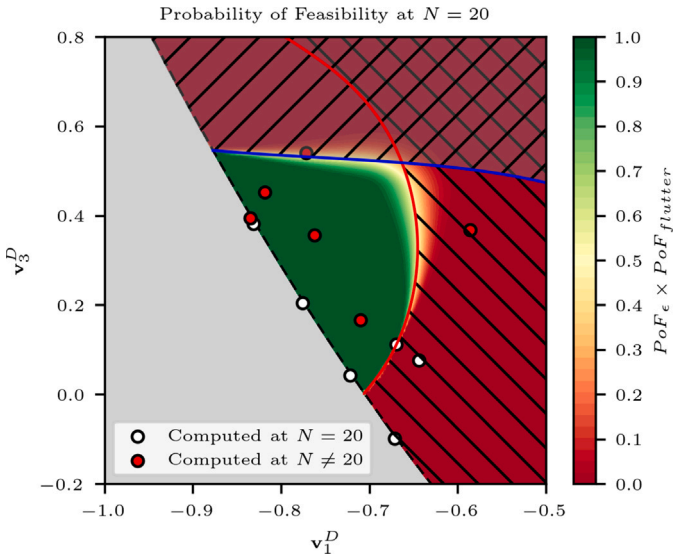

Fig. 7. Evolution of the Probability of Feasibility metric near the constraints. Green regions indicate feasible areas, while red regions denote areas where constraints are not satisfied.

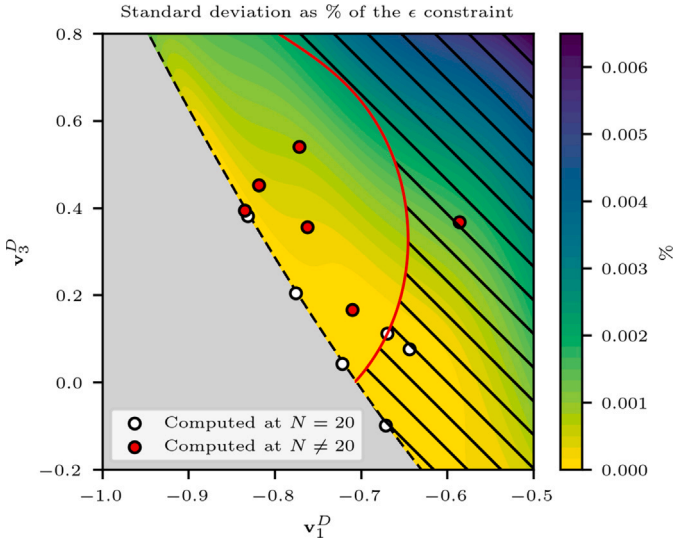

Fig. 8. Measure of accuracy for strain constraint's surrogate model, the isocontours represent the standard deviation of the constructed GPs.

where the constraints are not satisfied. The colour gradient between the two colours indicates how efficiently the surrogate models are capable of predicting the constraint value. For instance, the bottom region which has a higher concentration of study points shows a more abrupt behaviour than the top region where the computed points are further away.

An in-depth analysis of the surrogate model's accuracy at $N = 20$ plies is presented in Fig. 8, which depicts the standard deviation strain constraint. This plots is instrumental in understanding the constraints model accuracy in different regions of the design space. The plot is coherent with Fig. 7 given that the higher quality of the surrogate model depicts a more abrupt transition within the PoF metric. The colour differentiation between the computed points helps highlight the regions where the surrogate model demonstrates high precision, particularly around the white points. Remarkably, even the red points contribute positively to the construction of the surrogate model. The interplay between points at $N = 20$ and those from other layers underscores the comprehensive approach taken by the EGO process, ensuring that the surrogate model is well-defined not just in the immediate vicinity of the deterministic solution but also in the broader context of the design space.

Table 2
Error metrics for different surrogate modelling approaches in percentage of the design variable.

Surrogate model	ϵ_{eq} ε (%)	V_{flutt} ε (%)	M_x ε (%)
20 LHS	23.1	39.9	20.3
30 LHS	5.22	10.2	16.0
AK-MCS-10^2	1.12	5.49	2.60
AK-MCS-10^3	1.05	2.58	1.98
AK-MCS-10^4	0.537	0.174	0.351
EGO	**0.0466**	**0.225**	**0.228**

The detailed examination of the surrogate model's performance under varying conditions in the design space substantiates the effectiveness of the EGO approach in capturing aeroelastic responses with high fidelity, particularly in the context of optimising for a reduced number of plies while adhering to performance constraints. With the surrogate model now validated and proven to be sufficiently accurate, especially near the deterministic optimum and critical constraint boundaries, the research will now proceed to the Reliability-Based Design Optimisation (RBDO) phase. In this next phase, the established surrogate model will be instrumental in navigating the design space under probabilistic conditions.

4.1.1. Validation of the surrogate models

To validate the constructed surrogate models, we employed a MC approach to assess its accuracy near the optimum. A set of 100 points was generated within a circle of radius 0.1 in the $(\mathbf{v}_1^D, \mathbf{v}_3^D)$ space centred around the optimum. For each of these points, the actual values was computed and compared with the values predicted by the surrogate models. The differences between these values allowed us to estimate the error introduced by each surrogate model.

The validation was performed not only for our surrogate modelling strategy but also for several other ones for comparison:

- surrogate models created using only the initial DoE (20 LHS points);
- surrogate models created using 30 LHS points;
- three surrogate models created using our initial DoE but solving 10 iterations of the $EI \times PoF$ optimisation via Adaptive Kriging MC Simulation (AK-MCS) [44] with 100, 1000, and 10.000 points.

As a reminder, the proposed surrogate modelling strategy exploits an initial DoE of 20 LHS points, plus 9 points obtained from the infill function optimisation, Eq. (20).

Table 2 provides a quantitative summary of the mean error for each surrogate modelling strategy. The presented approach – $EI \times POF$ optimised via differential evolution – demonstrated a notable reduction in prediction errors, underscoring the efficacy of the EGO process in refining the surrogate model. The surrogate models created with 20 and 30 LHS points exhibited higher errors, reflecting the limitations of sparse sampling in capturing the complex aeroelastic responses. Meanwhile, the surrogate models optimised via AK-MCS showed varying degrees of accuracy depending on the number of points used in the optimisation process.

In conclusion, the validation process confirms that our surrogate model, developed using the EGO approach optimised via differential evolution, outperforms those created with traditional LHS methods and various AK-MCS configurations.

Table 3
Conditions and parameters of the GA-RBDO.

Parameter	Value
Population size	50
Mutation probability	0.5
Elitism group	10
N_{opt}	20
Standard deviation σ_θ	2°
MC samples	100.000
$\mathbb{P}_{limit}$	0.01

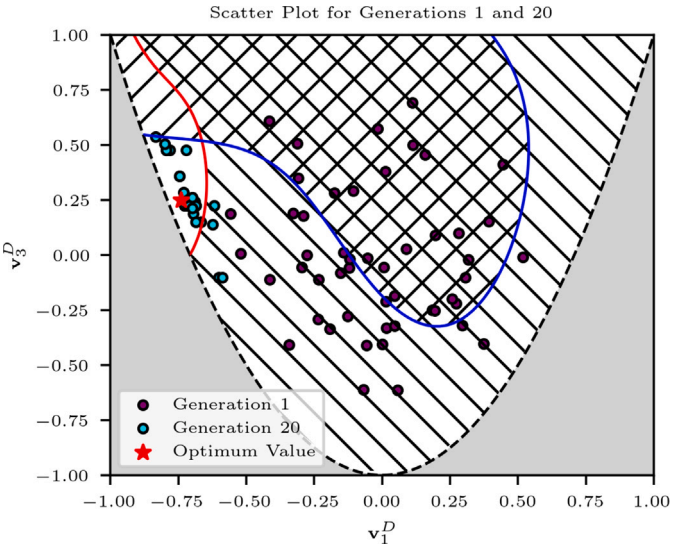

Fig. 9. Visualisation of the design space exploration by the GA, emphasising key areas of exploration and the optimal RBDO solution at 20 plies.

4.2. Reliability-based design optimisation outcomes

This phase focused on minimising gust response and number of plies, constrained by flutter speed and strain parameters, within a 2D space given a fixed ply count of 20. The RBDO employed a GA, rigorously designed to handle the inherent uncertainties in the ply orientation given by the fabrication processes.

To ensure the effectiveness and efficiency of the GA, it is imperative to fine-tune its parameters and operational conditions. The fine-tuning process involved iterative testing and validation against a set of benchmark problems, with adjustments made based on the performance metrics such as convergence rate and solution quality. Parameters such as population size, mutation rate, and crossover probability were adjusted in small increments, while monitoring the impact on the GA's ability to find optimal solutions within a reasonable timeframe. This iterative approach allowed us to identify the optimal settings that balance exploration and exploitation within the genetic algorithm framework. Table 3 summarises the key settings and values used in the GA, which were fine-tuned as described. All of these parameters were previously defined in detail in Section 3. Additionally, the table includes the standard deviation σ_θ, representing the variability introduced in the composite materials ply orientation, and the number of samples used in the MC analysis.

Exploration of the design space. Fig. 9 illustrates the exploration of the $(\mathbf{v}_1^D, \mathbf{v}_3^D)$ design space throughout two separate generations of a GA run, the first and the 22nd. The plot highlights the global initial exploration as well as areas of focused search and the distribution of solutions within the 22nd generation, including the optimal stacking sequence $\boldsymbol{\theta}_{optim}$ projection in the $(\mathbf{v}_1^D, \mathbf{v}_3^D)$ space. The images reflect the capability of the GA on exploring the design space and centring its attention as generation passes on the exploration of the zones near the fittest individuals.

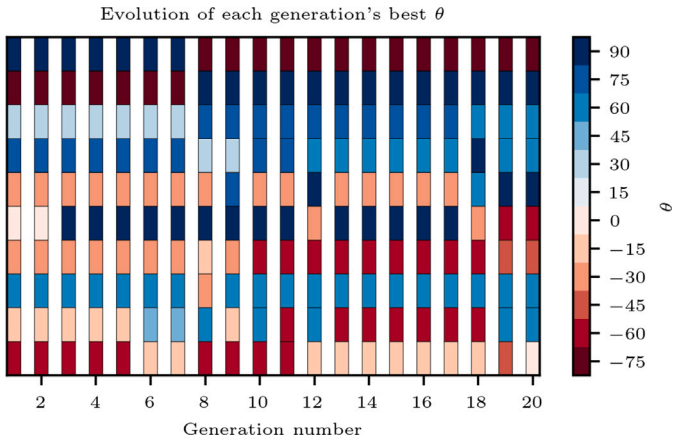

Fig. 10. Visualisation of the optimised stacking sequence determined by the RBDO at 20 plies, showcasing the ply orientations and ordering for a symmetrical θ.

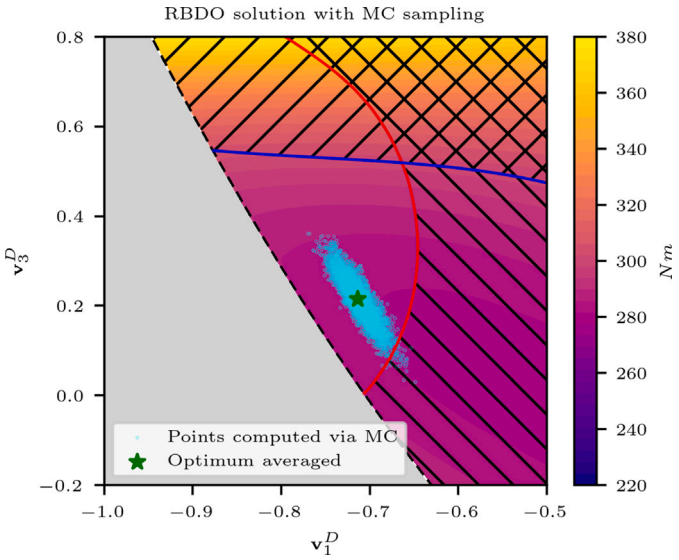

Fig. 11. Compliance of the optimised designs with probabilistic constraints on flutter speed and strain, achieved through GA optimisation at 20 plies.

Visualisation of the optimal stacking sequence. The optimal stacking sequence, resulting from the RBDO, is visualised in Fig. 10. This figure showcases the evolution of ply orientations and their specific order in the optimal design. It serves as a direct representation of the practical outcome of the optimisation process, highlighting the successful integration of material efficiency and structural performance. The plot also illustrates how the GA has not been capable of bettering the previous optimum stacking sequence at each iteration of the GA.

Probabilistic constraint compliance. The effectiveness of the RBDO in adhering to probabilistic constraints is demonstrated in Fig. 11. This plot shows how the optimised designs comply with the flutter speed and strain constraints while reducing the gust response shown within the isocontours. Within this plot we also added the entire MC sampling for the optimum individual to show how the failure probabilities where computed and illustrating how the failure probability constrained for the maximum static equivalent strain is respected.

Genetic algorithm convergence. The GA's convergence is of major importance in assessing the optimisation's reliability and efficiency. Fig. 12 presents the convergence plot of the algorithm, depicting the evolution of the optimisation over 30 generations. This plot encompasses the results from five separate runs of the algorithm, ensuring a thorough

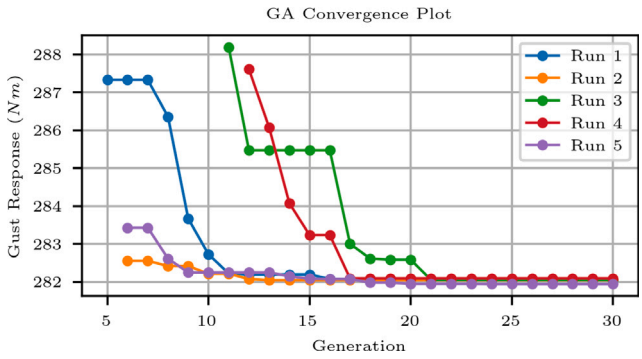

Fig. 12. Convergence plot of the gust response obtained with GA-RBDO, showing the optimisation progression over 30 generations. Consistency across five separate runs with different initial conditions underlines the algorithm robustness.

examination of its convergence behaviour. The consistency across these runs highlights the algorithm's robustness and reliability in finding an optimal solution, given that all the GA runs converged after a maximum of 21 iterations. Within Fig. 12, the value for the fittest individual which satisfies all probabilistic constraints is plotted. Given that only feasible individuals are plotted, the convergence lines do not start in generation 0 but in the first generation where a stacking sequence $\boldsymbol{\theta}$ satisfies all constraints. Run 5 found a feasible solution after only 5 generations, while other runs such as 3 and 4 took as much as 13 generations.

4.2.1. Validation of the final stacking sequence

The final stacking sequence has a probability of failure of only 0.771%, which is lower than the 1% upper limit, indicating a correct constraint compliance. This failure probability is determined using the modified MC simulation that accounts for the prediction error of the surrogate model (PoF), represented in Eq. (22). Without considering the PoF within the MC simulation, we would obtain a failure probability of 0.768%, indicating that the error induced by the surrogate model is only 0.003% and therefore a robust prediction of constraint compliance by the surrogate model. The small value obtained in surrogate model error certifies the robustness of the surrogate model construction and indicates a solid overall prediction of the constraint values, ensuring the reliability of the final stacking sequence. We note here that when other methodologies are used for the constraint evaluation, such as FORM or SORM [51,52], we do not have an indicator of the error of the surrogate model and we add also an error due to the inherent approximations on which these methodologies are based.

Moreover, a total of approximately 5.3×10^6 calls were made to the surrogate model during the optimisation process, for an average computational time of 35 min. To this computation time we must add the 29 initial points used to compute the surrogate model, each taking an average of 2 and a half minutes, giving a final computational time of approximately two hours for the whole optimisation.

Comparatively, a direct approach using the GA and the MC reliability estimator would require the same number of evaluation of the function of interests (5.3×10^6), but directly to the full order model. This would result – considering an average evaluation time of 2 and a half minutes – in a prohibitive optimisation time. Even if we would consider using a FORM/SORM estimator for the failure probability, a direct approach would require to call the full order model to construct the local approximation of the constraints for each point of the GA, and therefore a higher computational cost with respect to the proposed methodology.

These results collectively validate the efficacy of the surrogate model and the RBDO approach. The data-driven insights obtained emphasise the successful interplay between material savings and the reliability of aeroelastic performance, marking a significant advancement in the understanding and design of composite wing structures.

5. Conclusion

In this study, we presented a framework for the reliability-based optimisation of composite plates under aeroelastic constraints, integrating efficient global optimisation and genetic algorithms. Our methodology systematically combines surrogate modelling, homogenisation techniques, and probabilistic design to address the complexities inherent in composite material optimisation for aeroelastic applications.

The results underscore the effectiveness of the proposed approach in navigating the intricate design space of composite structures, achieving significant enhancements in performance and reliability. The application of surrogate models facilitated a nuanced understanding of the aeroelastic responses, enabling efficient exploration and optimisation within the lamination parameters design space. The genetic algorithm's robustness and adaptability were evident in its convergence behaviour and its ability to meet probabilistic constraints, yielding optimal stacking sequences that balance material efficiency with structural performance.

The integration of probabilistic design considerations marks a major advancement, ensuring that the optimised composite structures not only meet performance criteria but also adhere to safety and reliability standards under manufacturing variability. This approach aligns with the industry's move towards more sustainable and efficient designs and paves the way for further advancements in composite material optimisation techniques. While this study is specifically applied to aeroelastic tailoring, the proposed optimisation framework is versatile and can be extended to other RBDO problems in composite structures, including those involving buckling and strength constraints. This flexibility notes the robustness and efficiency of our methodology in handling diverse optimisation scenarios with expensive cost functions.

Future work could extend this framework to encompass more complex structures and loading conditions, integrate machine learning techniques for improved surrogate model accuracy for efficient uncertainty quantification and data assimilation techniques [53], and explore alternative optimisation algorithms for enhanced efficiency. Additionally, while this study focuses on a linear mechanics scenario, it is important to note that the proposed methodology is fully capable of incorporating geometrical nonlinearities. The Kriging surrogate models used in our approach are nonlinear and can effectively capture the behaviour of structures under large deformations. The continued development of these methodologies holds great promise for advancing the state of the art in composite material design, particularly in the aerospace sector.

In conclusion, this study offers a significant contribution to the field of composite material optimisation, providing a robust and efficient framework for designing more reliable and efficient composite structures. The insights gained from this research not only demonstrate the potential of integrating advanced optimisation techniques and probabilistic approaches but also lay the groundwork for future innovations in aerospace composite design.

CRediT authorship contribution statement

Roger Ballester Claret: Writing – original draft, Visualization, Software, Methodology, Investigation, Formal analysis, Data curation, Conceptualization. **Ludovic Coelho:** Writing – review & editing, Methodology, Conceptualization. **Christian Fagiano:** Writing – review & editing, Supervision, Methodology, Formal analysis, Conceptualization. **Cédric Julien:** Writing – review & editing, Supervision, Methodology, Formal analysis, Conceptualization. **Didier Lucor:** Writing – review & editing, Supervision, Methodology, Formal analysis, Conceptualization. **Nicolò Fabbiane:** Writing – review & editing, Supervision, Project administration, Methodology, Funding acquisition, Formal analysis, Conceptualization.

Declaration of competing interest

The authors declare the following financial interests/personal relationships which may be considered as potential competing interests: Roger Ballester Claret reports financial support was provided by French National Aerospace Research Centre. If there are other authors, they declare that they have no known competing financial interests or personal relationships that could have appeared to influence the work reported in this paper.

Data availability

Data will be made available on request.

Acknowledgements

This research was made possible through the funding of Roger Ballester Claret's thesis provided by the General Scientific Direction of ONERA, France.

References

[1] Munk M. Propeller containing diagonally disposed fibrous material. 1949, Patent issued October 11, 1949. U.S. Patent No. 2, 484, 308.
[2] Weisshaar T. Aeroelastic tailoring of forward swept composite wings. J Aircr 1981;18(8):669–76.
[3] Jutte C, Stanford B. Aeroelastic tailoring of transport aircraft wings: State-of-the-art and potential enabling technologies. Technical report NASA/TM-2014-218252, NASA; 2014.
[4] Irisarri F-X, Lasseigne A, Leroy F-H, Le Riche R. Optimal design of laminated composite structures with ply drops using stacking sequence tables. Compos Struct 2014;107:559–69.
[5] Ghiasi H, Fayazbakhsh K, Pasini D, Lessard L. Optimum stacking sequence design of composite materials part II: Variable stiffness design. Compos Struct 2010;93(1):1–13. http://dx.doi.org/10.1016/j.compstruct.2010.06.001.
[6] Miki M, Sugiyama Y. Optimum design of laminated composite plates using lamination parameters. AIAA J 1993;31:921–2. http://dx.doi.org/10.2514/3.49033.
[7] Tsai SW, Halpin JC, Pagano NJ. Composite materials workshop. Stamford, CT: Technomic Pub. Co.; 1968, p. 233–5.
[8] Setoodeh S, Abdalla MM, Gürdal Z. Design of variable–stiffness laminates using lamination parameters. Composites B 2006;37(4):301–9. http://dx.doi.org/10.1016/j.compositesb.2005.12.001.
[9] Gürdal G, Haftka RT, Hajela P. Design and optimization of laminated composite materials. New York: Wiley; 1999.
[10] Irisarri F-X, Julien C, Bettebghor D, Lavelle F, Guerin Y, Mathis K. A general optimization strategy for composite sandwich structures. Struct Multidiscip Optim 2021;63:3027–44, Published online: 15 February 2021.
[11] Lucor D, Enaux C, Jourdren H, Sagaut P. Stochastic design optimization: Application to reacting flows. Comput Methods Appl Mech Engrg 2007;196(49–52):5047–62.
[12] Sriramula S, Chryssanthopoulos MK. Quantification of uncertainty modelling in stochastic analysis of FRP composites. Composites A 2009;40(11):1673–84. http://dx.doi.org/10.1016/j.compositesa.2009.08.020.
[13] Potter K, Khan B, Wisnom M, Bell T, Stevens J. Variability, fibre waviness and misalignment in the determination of the properties of composite materials and structures. Composites A 2008;39(9):1343–54. http://dx.doi.org/10.1016/j.compositesa.2008.04.016.
[14] Pettit CL. Uncertainty quantification in aeroelasticity: Recent results and research challenges. J Aircr 2004;41(5):1217–29. http://dx.doi.org/10.2514/1.3961.
[15] An H, Youn BD, Kim HS. Reliability-based design optimization of laminated composite structures under delamination and material property uncertainties. Int J Mech Sci 2021;205:106561. http://dx.doi.org/10.1016/j.ijmecsci.2021.106561.
[16] Lopez R, Beck A. Reliability-based design optimization strategies based on FORM: a review. J Braz Soc Mech Sci Eng 2012;34(4):506–14. http://dx.doi.org/10.1590/S1678-58782012000400012.
[17] Lu L, Wu Y, Zhang Q, Qiao P. A transformation-based improved kriging method for the black box problem in reliability-based design optimization. Mathematics 2023;11(1):218. http://dx.doi.org/10.3390/math11010218, Received: 29 November 2022; Revised: 26 December 2022; Accepted: 28 December 2022; Published: 1 January 2023.
[18] Li X, Yang Q, Wang Y, Han X, Cao Y, Fan L, Ma J. Development of surrogate models in reliability-based design optimization: A review. Math Biosci Eng 2021;18(5):6386–409. http://dx.doi.org/10.3934/mbe.2021317, Received: 27 May 2021; Accepted: 06 July 2021; Published: 21 July 2021.
[19] Kuschel N, Rackwitz R. Two basic problems in reliability-based structural optimization. Math Methods Oper Res 1997;46(3):309–33. http://dx.doi.org/10.1007/BF01194859.
[20] Reddy M, Grandhi R, Hopkins D. Reliability-based structural optimization: a simplified safety index approach. Comput Struct 1994;53(6):1407–18.
[21] Coelho L, Lucor D, Fabbiane N, Fagiano C, Julien C. Multi-scale approach for reliability-based design optimization with metamodel upscaling. Struct Multidiscip Optim 2023;66(205). http://dx.doi.org/10.1007/s00158-023-03643-4.
[22] Jones DR, Schonlau M, Welch WJ. Efficient global optimization of expensive black-box functions. J Global Optim 1998;13:455–92, Printed in the Netherlands.
[23] Sabater C, Bekemeyer P, Görtz S. Efficient bilevel surrogate approach for optimization under uncertainty of shock control bumps. AIAA J 2020;58(12).
[24] Xu W, Jiang Y, Svetozarevic B, Jones CN. Constrained efficient global optimization of expensive black-box functions. 2023, http://dx.doi.org/10.48550/arXiv.2211.00162, Accepted to ICML 2023. arXiv:2211.00162.
[25] Pelamatti J, Brevault Lc, Balesdent M, Talbi E-G, Guerin Y. Efficient global optimization of constrained mixed variable problems. J Glob Optim 2019;73. Published online: 30 November 2018.
[26] Scarth C, Cooper JE. Reliability-based aeroelastic design of composite plate wings using a stability margin. Struct Multidiscip Optim 2018;57:1695–709. http://dx.doi.org/10.1007/s00158-017-1838-6, Open access.
[27] Fabbiane N, Irisarri F-X, Dillinger J, Lepage A. Aeroelastic-tailoring of a wind-tunnel model for passive alleviation of static and dynamic loads. CEAS Aeronaut J 2022;13(4):967–77. http://dx.doi.org/10.1007/s13272-022-00615-0.
[28] Isaaks EH, Srivastava RM. An introduction to applied geostatistics. New York: Oxford University Press; 1989.
[29] Kameyama M, Fukunaga H. Optimum design of composite plate wings for aeroelastic characteristics using lamination parameters. Comput Struct 2007;85(3–4):213–24.
[30] Kim T-U, Hwang IH. Optimal design of composite wing subjected to gust loads. Comput Struct 2005;83(19–20):1546–54.
[31] Oh D, Librescu L. Free vibration and reliability of composite cantilevers featuring uncertain properties. Reliab Eng Syst Saf 1997;56(3):265–72.
[32] Rodden WP, Taylor PF, McIntosh J. Further refinements of the nonplanar aspects of the subsonic doublet-lattice lifting surface method. In: Proceedings of the international council of the aeronautical sciences. 1996, p. 1786–99, Paper 96-2.8.2.
[33] Hassig HJ. An approximative true damping solution of the flutter equation by determinant iteration. J Aircr 1971;8(11):885–9.
[34] Bailie JA, Ley RP, Pasricha A. Summary and review of composite laminate design guidelines. Tech. rep., Northrop Grumman Corporation, Military Aircraft Systems Division; 1997, NASA Contract NAS1-19347, Final Report June 1997 – October 1997.
[35] IJsselmuiden S, Abdalla M, Gürdal Z. Implementation of strength-based failure criteria in the lamination parameter design space. AIAA J 2008;46(7):1826–34. http://dx.doi.org/10.2514/1.35565.
[36] Catapano A, Montemurro M. On the correlation between stiffness and strength properties of anisotropic laminates. Mech Adv Mater Struct 2019;26(8):651–60. http://dx.doi.org/10.1080/15376494.2017.1410906.
[37] Montemurro M, Catapano A, Doroszewski D. A multi-scale approach for the simultaneous shape and material optimisation of sandwich panels with cellular core. Composites B 2016;91:458–72. http://dx.doi.org/10.1016/j.compositesb.2016.01.030.
[38] Queipo NV, Haftka RT, Shyy W, Goel T, Vaidyanathan R, Tucker PK. Surrogate-based analysis and optimization. Prog Aerosp Sci 2005;41(1):1–28.
[39] Saves P, Lafage R, Bartoli N, Diouane Y, Bussemaker J, Lefebvre T, Hwang JT, Morlier J, Martins JRRA. SMT 2.0: A surrogate modeling toolbox with a focus on hierarchical and mixed variables Gaussian processes. Adv Eng Sofw 2024;188:103571. http://dx.doi.org/10.1016/j.advengsoft.2023.103571.
[40] McKay M, Beckman R, Conover W. A comparison of three methods for selecting values of input variables in the analysis of output from a computer code. Technometrics 1979;21:239–45.
[41] Storn R, Price K. Differential evolution – A simple and efficient heuristic for global optimization over continuous spaces. J Global Optim 1997;11(4):341–59. http://dx.doi.org/10.1023/A:1008202821328, Published: December 1997.
[42] Coma M, Monshi Tousi N, Pons-Prats J, Bugeda G, Bergada JM. A new hybrid optimization method, application to a single objective active flow control test case. Appl Sci 2022;12(8):3894. http://dx.doi.org/10.3390/app12083894.
[43] Lee D, Gonzalez L, Periaux J, Srinivas K, Onate E. Hybrid-game strategies for multi-objective design optimization in engineering. Comput & Fluids 2011;47:189–204, [CrossRef].
[44] Li P, Wang Y. An active learning reliability analysis method using adaptive Bayesian compressive sensing and Monte Carlo simulation (ABCS-MCS). Reliab Eng Syst Saf 2022;221:108377. http://dx.doi.org/10.1016/j.ress.2022.108377.
[45] Durantin C, Marzat J, Balesdent M. Analysis of multi-objective kriging-based methods for constrained global optimization. Comput Optim Appl 2016;63:903–26, Published online: 14 September 2015.

[46] Schonlau M, Welch WJ, Jones DR. Global versus local search in constrained optimization of computer models. In: New developments and applications in experimental design. Lecture notes-monograph series, vol. 34, Institute of Mathematical Statistics; 1998, p. 11–25.

[47] Soremekun G, Gürdal Z, Kassapoglou C, Toni D. Stacking sequence blending of multiple composite laminates using genetic algorithms. Compos Struct 2002;56(1):53–62.

[48] Liu W-S, Cheung SH, Cao W-J. An efficient surrogate-aided importance sampling framework for reliability analysis. Adv Eng Softw 2019;135:102687. http://dx.doi.org/10.1016/j.advengsoft.2019.102687.

[49] Ababou R, Bagtzoglou AC, Wood EF. On the condition number of covariance matrices in kriging, estimation, and simulation of random fields. Math Geol 1994;26:99–133. http://dx.doi.org/10.1007/BF02065878.

[50] Kraft D. A software package for sequential quadratic programming. Deutsche forschungs- und versuchsanstalt für luft- und raumfahrt köln: forschungsbericht, vol. 88, Number 28, Köln: Wiss. Berichtswesen d. DFVLR; 1988, p. 33.

[51] Bjerager P. Probability computation methods in structural and mechanical reliability. In: Liu W, Belytscko T, editors. Computational mechanics of probabilistic and reliability analysis. Lausanne, Switzerland: Elmepress International; 1991, p. 49–67.

[52] Cizelj L, Mavko B, Riesch-Oppermann H. Application of first and second order reliability methods in the safety assessment of cracked steam generator tubing. Nucl Eng Des 1994;147.

[53] Cheng S, Quilodrán-Casas C, Ouala S, Farchi A, Liu C, Tandeo P, Fablet R, Lucor D, Iooss B, Brajard J, et al. Machine learning with data assimilation and uncertainty quantification for dynamical systems: a review. IEEE/CAA J Autom Sin 2023;10(6):1361–87.